



---

Supplementary Materials

# Enhanced Metal-Support Interaction in Ni/Biomass-Derived Carbon Catalyst via Atomic Ni-N<sub>4</sub> Sites for Boosting Dye-Sensitized Photocatalytic H<sub>2</sub> Production

Weiying Zhang \*, Qi Wu, Tian Liao, Niuniu Guo, Shiyu Liu, Shaoqin Peng and Yuexiang Li \*

Key Laboratory of Jiangxi Province for Environment and Energy Catalysis, School of Chemistry and Chemical Engineering, Nanchang University, Nanchang 330010, China; 15707900685@163.com (T.L.); xtt11012025@163.com (N.G.); 18770547570@163.com (S.L.); pengshaoqin@ncu.edu.cn (S.P.)

\* Correspondence: zhangwy@ncu.edu.cn (W.Z.); liyx@ncu.edu.cn (Y.L.)

---

## Characterization

The adsorption amount of EY on different samples was tested as follows: 20 mg APC or x-Ni/APC composite catalyst was added to 100 mL of EY solution ( $1 \times 10^{-5}$  mol L<sup>-1</sup>), kept stirring for 2 h. Then the dispersion was centrifugated at 9000 rpm for 5 min twice to ensure that there was no solid residue. The absorbance of the supernate was measured on a UV-vis spectrophotometer (Hitachi U3310, Japan). The adsorption amount was calculated according to the concentration difference.

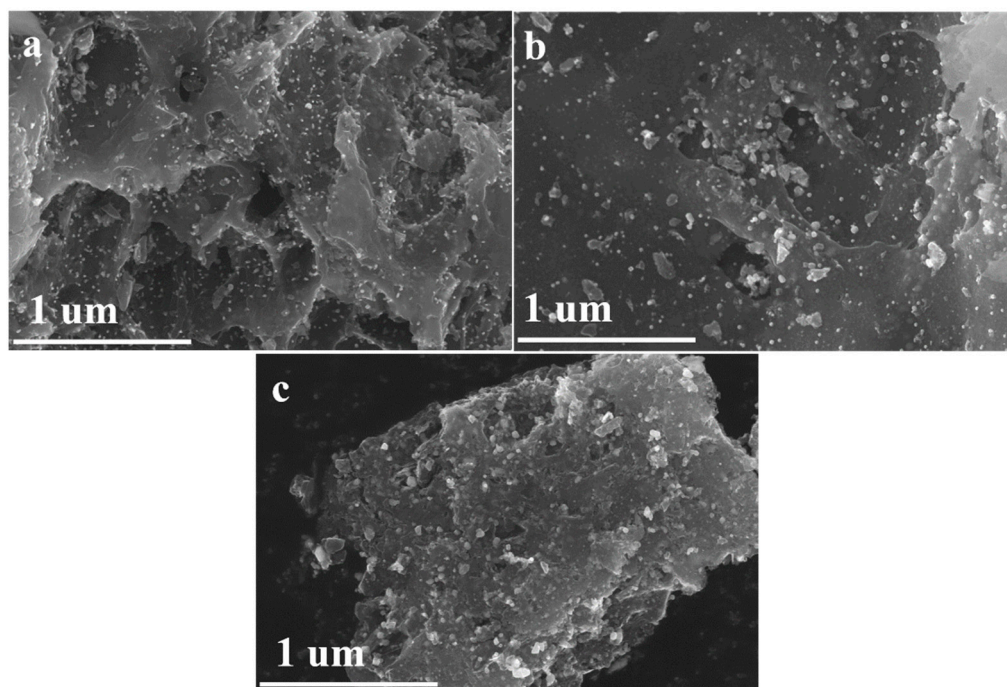


Figure S1. SEM images for (a) 1-Ni/APC, (b) 2-Ni/APC, and (c) 3-Ni/APC composites.

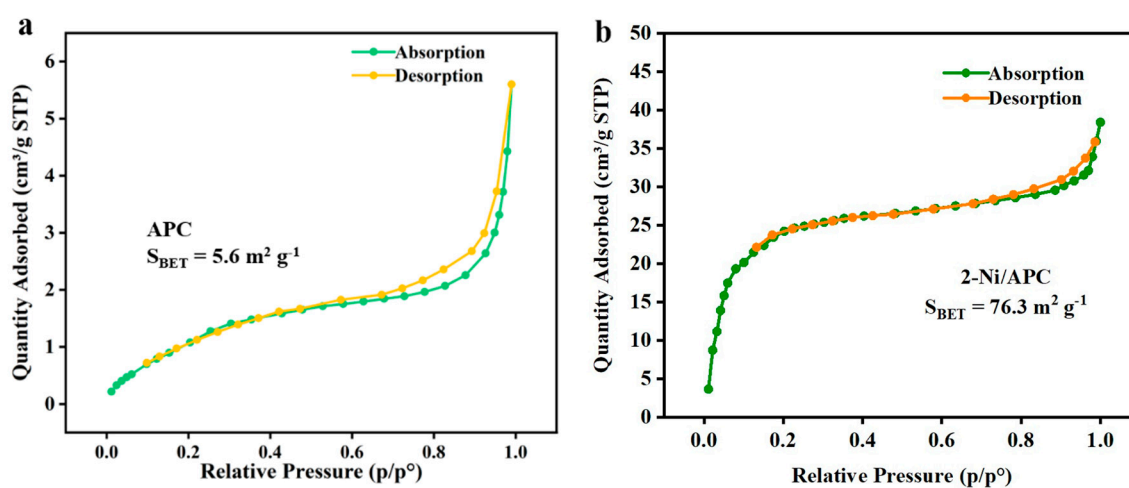


Figure S2.  $\text{N}_2$  adsorption-desorption isotherms of (a) APC and (b) 2-Ni/APC.

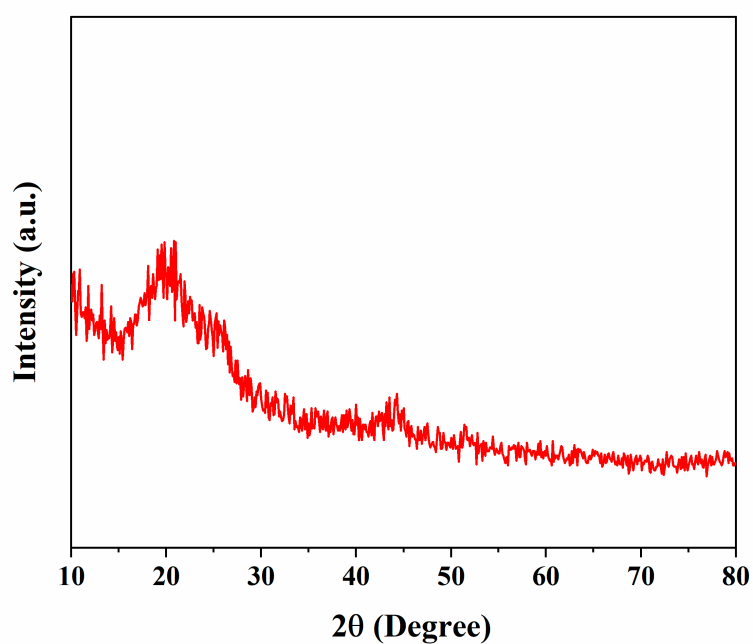


Figure S3. XRD pattern of T-2-Ni/APC.

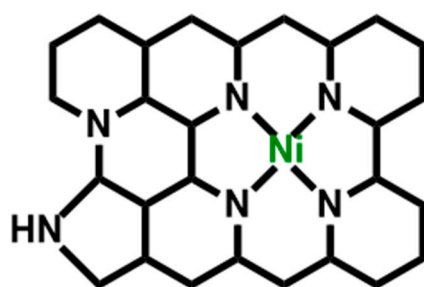


Figure S4. The diagram of Ni-N<sub>4</sub> structure.

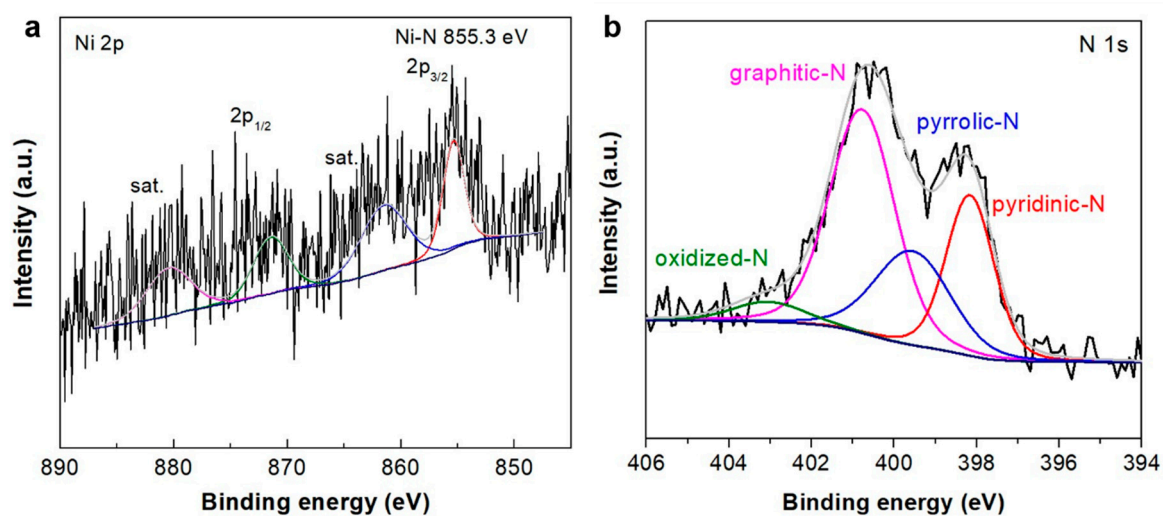
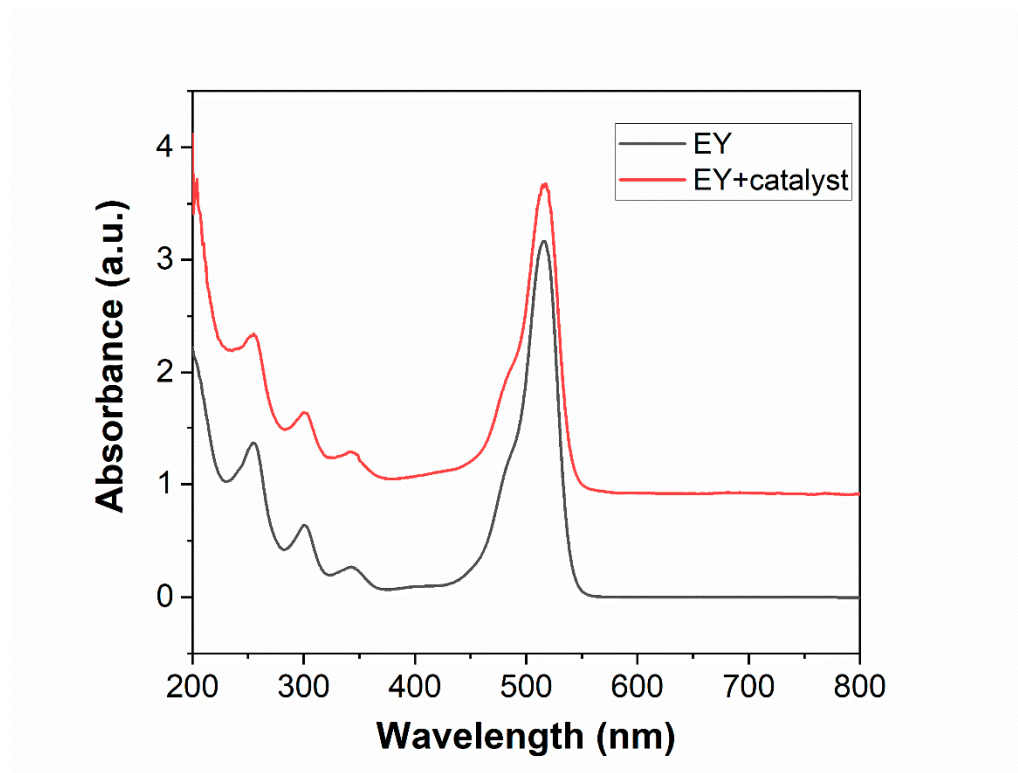
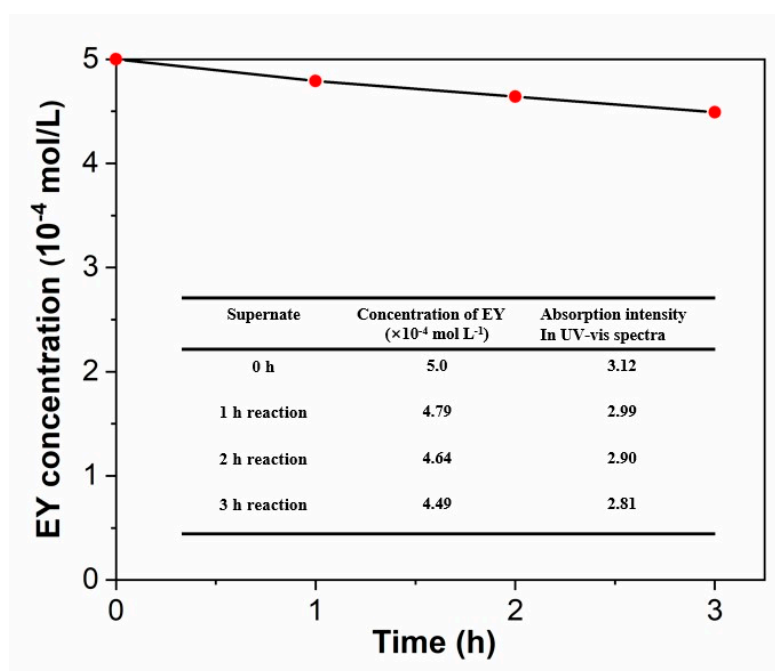


Figure S5. (a) Ni 2p and (b) N 1s spectra of T-2-Ni/APC sample.



**Figure S6.** UV-vis spectra of pure EY, and EY + catalyst (2-Ni/APC) system in the reaction solution. EY:  $5 \times 10^{-4}$  mol L<sup>-1</sup>; catalyst: 100 mg.



**Figure S7.** The dye degradation rate during a 3 h cycle stability test. The EY concentration was measured by using UV-vis spectra according to the absorption intensity variation after different illumination times.

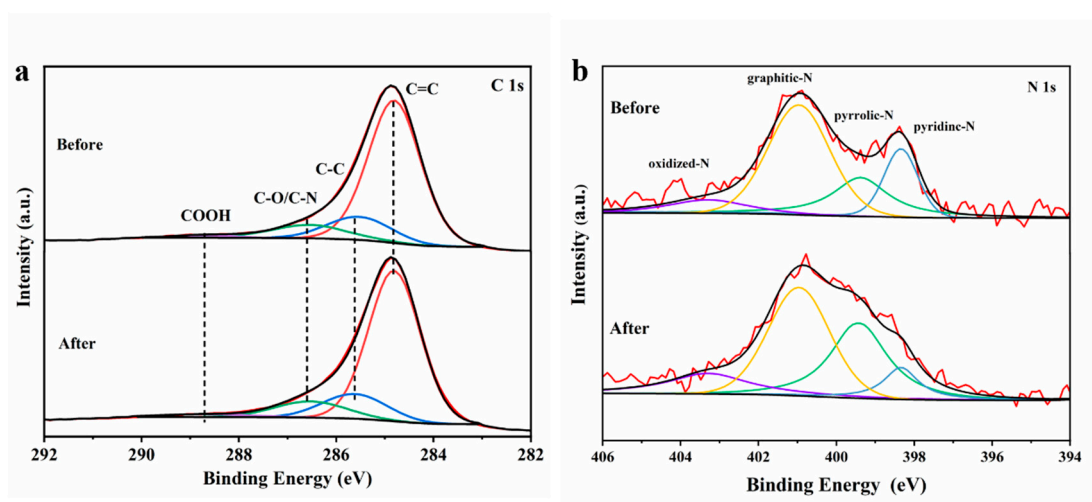


Figure S8 (a) C 1s and (b) N 1s spectra for fresh and cycled 2-Ni/APC composite.

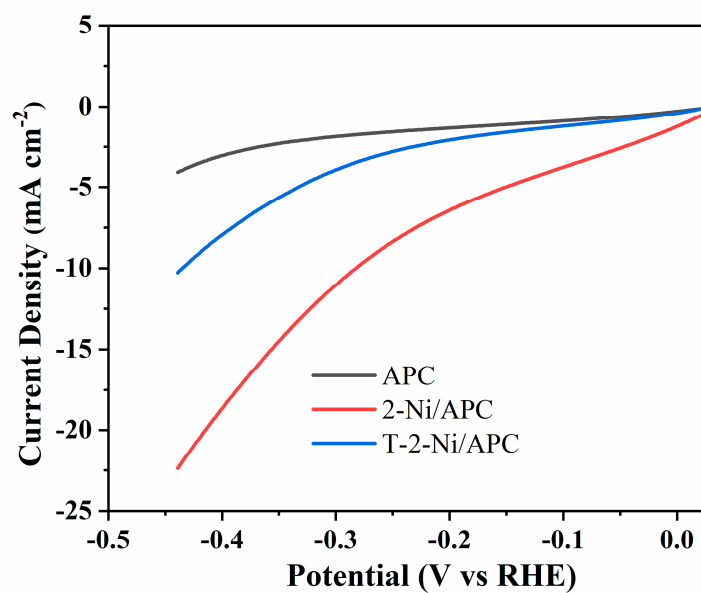
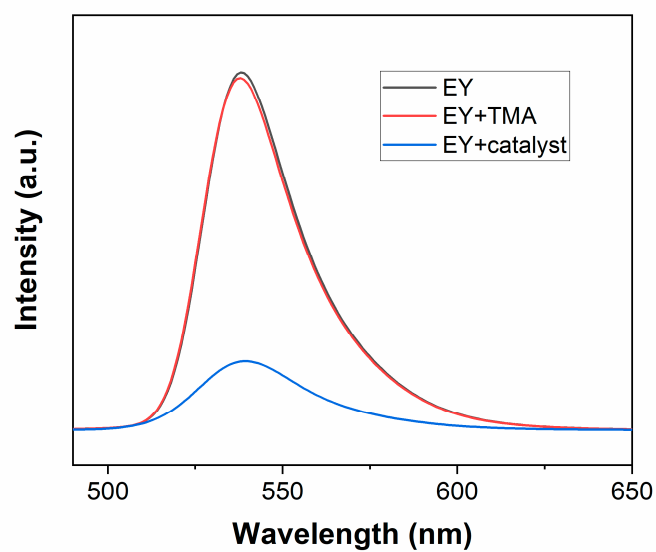
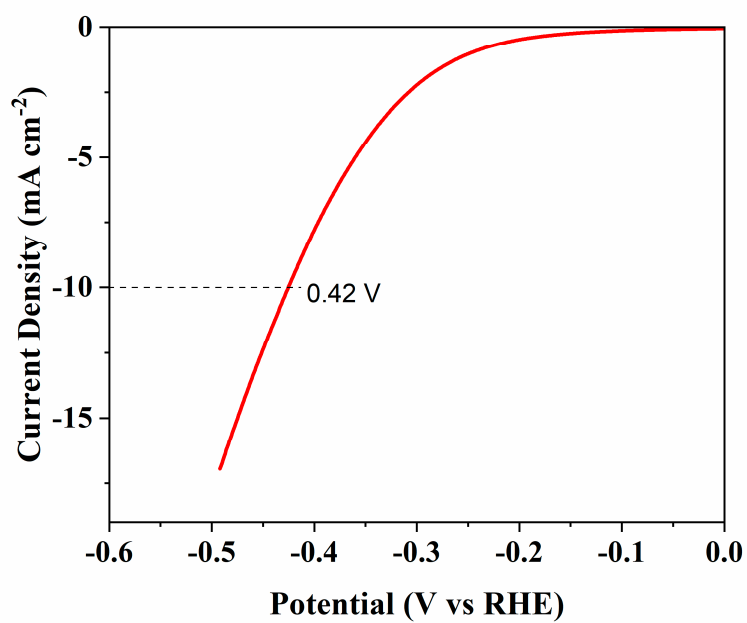


Figure S9. LSV curves of APC, 2-Ni/APC, and T-2-Ni/APC in 1.0 M KOH solution.



**Figure S10.** Fluorescence spectra of EY, EY+TMA, and EY+catalyst (2-Ni/APC) systems. EY:  $5 \times 10^{-4}$  mol L<sup>-1</sup>; TMA:  $7.7 \times 10^{-2}$  mol L<sup>-1</sup>; catalyst: 100 mg; excitation wavelength: 450 nm.



**Figure S11.** LSV curve of T-2-Ni/APC in 0.5 M H<sub>2</sub>SO<sub>4</sub> solution.

**Table S1** Parameters for the calculation of AQY under different illumination conditions.

<b>Wavelength (nm)</b>	<b>420</b>	<b>450</b>	<b>470</b>	<b>520</b>	<b>600</b>
Illumination intensity (mW cm <sup>-2</sup> )	17.45	17.85	14.33	16.93	18.24
H <sub>2</sub> evolution (μmol)	30.70	38.86	23.21	19.62	0.25

AQY is calculated based on the detailed equation below:

$$AQY = \frac{2nN_Ahc}{Ist\lambda} \quad (1)$$

Where  $n$  is the mole of produced H<sub>2</sub>,  $N_A$  is the Avogadro's constant,  $h$  is the Planck constant,  $c$  is the speed of light,  $I$  is the illumination intensity,  $s$  is the area of light spot ( $r = 0.5$  cm),  $t$  is the illumination time (1 h),  $\lambda$  is the wavelength of light.



**Table S2.** Comparison of dye-sensitization photocatalytic hydrogen production activities for different carbon-based catalysts.

NO.	System	Reaction conditions	AQY (%) for H <sub>2</sub> evolution activity	Ref.
1	EY-Ni/agaric-derived porous carbon	$\lambda \geq 420$ nm, TMA, pH=11.0	41.0 % at $\lambda=450$ nm	This work
2	EY-Co(OH) <sub>2</sub> /GR	$\lambda \geq 420$ nm, TEOA	12.8 % at $\lambda=520$ nm	53
3	EY-CoP/g-C <sub>3</sub> N <sub>4</sub>	$\lambda \geq 420$ nm, TMA, pH=10.0	56.3 % at $\lambda=420$ nm	54
4	EY-graphdiyne/CuBr	$\lambda \geq 420$ nm, TEOA, pH=10.0	5.86 % at $\lambda=550$ nm	55
5	EY-NiO/rGO	$\lambda \geq 420$ nm, TEOA, pH=10.0	39.4 % at $\lambda=420$ nm	56
6	EY-NiCu/rGO	$\lambda \geq 420$ nm, TMA, pH=11.0	67.7 % at $\lambda=420$ nm	12
7	EY-Co/Co(OH) <sub>2</sub> /RGO	$\lambda \geq 420$ nm, TMA, pH=11.0	20.1 % at $\lambda=420$ nm	1
8	EY-UiO-66@g-C <sub>3</sub> N <sub>4</sub> /Ni	$\lambda \geq 420$ nm, TEOA, pH=7.0	6.41 % at $\lambda=420$ nm	57
9	EY-Co(OH) <sub>3</sub> Cl/rGO	$\lambda \geq 420$ nm, TMA, pH=10.0	28.3 % at $\lambda=420$ nm	58
10	EY-C-CuO(Hollow)/HSs	$\lambda \geq 420$ nm, TEOA, pH=7.0	25.3 % at $\lambda=520$ nm	59
11	EY-Ni/rGO	$\lambda \geq 420$ nm, TMA, pH=10.0	47.7 % at $\lambda=470$ nm	7
12	TiO <sub>2</sub> /WO <sub>3</sub> /corn straw-based graphene-like	$\lambda \geq 365$ nm, TEOA	0.32 % at $\lambda=365$ nm	60
13	EY-NiS@NC/CdS	$\lambda \geq 365$ nm, TEOA	0.66 % at $\lambda=365$ nm	61
14	EY-MoS <sub>3</sub> /AuNP/rGO	$\lambda \geq 400$ nm, TEOA	8.6 % at $\lambda=520$ nm	62
15	EY-MoSSe@rGO	$\lambda \geq 420$ nm, TEOA	6.8 % at $\lambda=420$ nm	63

## References

- Zhang, W.Y.; Ai, P.; Yuan, L.W.; Peng, S.Q.; Li, Y.X. In-situ converting CoO@Co/RGO into Co/Co(OH)<sub>2</sub>/RGO for improved dye-sensitized photocatalytic H<sub>2</sub> evolution. *Fuel* **2024**, *369*, 31785.
- Zhang, W.Y.; Peng, S.Q.; Li, Y.X. Template-free synthesis of hollow Ni/reduced graphene oxide composite for efficient H<sub>2</sub> evolution. *J. Mater. Chem. A* **2017**, *5*, 13072–13078.
- Zhang, W.Y.; Mei, X.; Yuan, L.W.; Wang, G.; Li, Y.X.; Peng, S.Q. Tuning metal-support interaction of NiCu/graphene cocatalysts for enhanced dye-sensitized photocatalytic H<sub>2</sub> evolution. *Appl. Surf. Sci.* **2022**, *593*, 153459.
- Y. Wei, J.G. Hao, J.L. Zhang, et al., Integrating Co(OH)<sub>2</sub> nanosheet arrays on graphene for efficient noble-metal-free EY-sensitized photocatalytic H<sub>2</sub> evolution. *Dalton T.* **52** (2023) 13923-13929.
- S.Q. Peng S, X. Huang, Y. Cao, et al., Modification of carbon nitride with noble-metal-free cobalt phosphide for effective photocatalytic hydrogen evolution. *Appl. Surf. Sci.* **584** (2022) 152610.
- J.K. Li, M. Li, H.Y. Li, et al., Novel CuBr-assisted graphdiyne synthesis strategy and application for efficient photocatalytic hydrogen evolution. *J. Mater. Chem. C* **10** (2022) 2181-2193.
- W.Y. Zhang, Z. Li, H. Li, et al., Facile synthesis of amorphous NiO/reduced graphene oxide as a cocatalyst for enhanced dye-sensitized photocatalytic H<sub>2</sub> evolution. *Energy Fuels* **36** (2022) 15112-15119.
- A. Jamma, B. Jaksani, C.S. Vennapoosa, et al., Defect-rich UiO-66@g-C<sub>3</sub>N<sub>4</sub>/Ni frameworks as efficient water splitting photocatalysts. *Mater. Adv.* **5** (2024) 2785-2796.

- 
- 58 W.Y. Zhang, Y.L. Zou, X. Mei, et al. Facile synthesis of  $\text{Co}_2(\text{OH})_3\text{Cl}$ /cobalt carbide/reduced graphene oxide composites for enhanced dye-sensitized photocatalytic  $\text{H}_2$  evolution. *Sustain. Energ. Fuels* 4 (2020) 6181-6187.
- 59 F.L. Wang, L.H. Xiao, J.M. Chen, et al., Regulating the electronic structure and water adsorption capability by constructing carbon-doped CuO hollow spheres for efficient photocatalytic hydrogen evolution. *ChemSusChem* 13 (2020) 5711-5721.
- 60 M. Sun, Y.L. Zhou, B. Sun, et al., Preparation of  $\text{TiO}_2/\text{WO}_3$ -corn straw-based graphene-like composite and its low light catalytic hydrogen production performance and mechanism. *Fuel* 343 (2023) 127936.
- 61 D.S. Xu, J. Ke, Z.Y. Yan, et al. Unveiling ternary  $\text{NiS@NC/CdS}$  heterojunction synergistically induced superior photo/electrocatalytic hydrogen evolution. *Appl. Catal. B-Environ. Energy* 362 (2025) 124746.
- 62 B. Vedhanarayanan, C.C. Chen, T.W. Lin, Plasmon-enhanced photocatalytic hydrogen production by dual dye sensitized ternary composite of  $\text{MoS}_3/\text{Au}$  core-Ag shell nanoparticles/graphene, *J. Power Sources* 477 (2020) 229033.
- 63 K. Namsheer, K. Pramoda, K.S.S. Kumar, et al., Molybdenum sulfo-selenide nanocomposites with carbon nanotubes and reduced graphene oxide for photocatalytic hydrogen evolution reaction. *Energy Adv.* 2 (2023) 1724-1734.